International Journal of Heat and Mass Transfer 65 (2013) 62–72

Contents lists available at SciVerse ScienceDirect

International Journal of Heat and Mass Transfer

journal homepage: www.elsevier.com/locate/ijhmt

Volume of fluid-based numerical modeling of condensation heat transfer and fluid flow characteristics in microchannels

H. Ganapathy [a], A. Shooshtari [a], K. Choo [a], S. Dessiatoun [a], M. Alshehhi [b], M. Ohadi [a,*]

[a] Department of Mechanical Engineering, University of Maryland, College Park, MD 20742, USA
[b] Department of Mechanical Engineering, The Petroleum Institute, P.O. Box 2533, Abu Dhabi, United Arab Emirates

ARTICLE INFO

Article history:
Received 9 November 2012
Received in revised form 30 April 2013
Accepted 16 May 2013
Available online 26 June 2013

Keywords:
Condensation
Microchannel
Numerical simulation
Volume of fluid
Flow patterns

ABSTRACT

The present work proposes a numerical model for the simulation of condensation heat transfer and fluid flow characteristics in a single microchannel. The model was based on the volume of fluid approach, which governed the hydrodynamics of the two-phase flow. The condensation characteristics were governed by the physics of the phenomena and did not include any empirical expressions in the formulation. The conventional governing equations for conservation of volume fraction and energy were modified to include source terms that accounted for the mass transfer at the liquid–vapor interface and the associated release of latent heat, respectively. A microchannel having characteristic dimension of 100 μm was modeled using a two-dimensional computational domain. The working fluid was R134a and the vapor mass flux at the channel inlet ranged from 245 to 615 kg/m^2 s. The channel wall was maintained at a constant heat flux ranging from 200 to 800 kW/m^2. The predictive accuracy of the numerical model was assessed by comparing the two-phase frictional pressure drop and Nusselt number with available empirical correlations in the literature. A reasonably good agreement was obtained for both parameters with a mean absolute error of 8.1% for two-phase frictional pressure drop against a recent universal predictive approach, and 16.6% for Nusselt number against an available correlation. Further, a qualitative comparison of various flow patterns against experimental visualization data also indicated a favorable agreement.

1. Introduction

Miniaturization of electronic devices has led to advances in various engineering fields, including space technology, defense systems, aerospace applications, manufacturing technology, industrial processes and consumer electronics. Researchers in these fields are investigating ways to manage the thermal dissipation from electronic components in miniaturized devices, with the aim of guaranteeing the reliability and safety of the device during operation. The use of microscale heat exchangers to manage this thermal dissipation has been widely studied since the pioneering work of Tuckerman and Pease [1]. Since then, majority of the literature has focused on characterizing the heat transfer coefficient and pressure drop for electronics cooling applications, as reported by Sobhan and Garimella [2]. While changes in simple channel geometries can yield significant enhancements in thermal performance, the improvements come at the expense of high pressure drops. However, this drawback is being actively mitigated by the development of advanced designs for microchannel heat exchangers, using innovative fluid feed systems (Ohadi et al. [3], Kim et al. [4]).

A major advantage of numerical modeling of heat transfer over simpler empirical correlation-based approaches is that, the former, when appropriately validated with experimental data, may serve as an effective tool for the design and optimization of next-generation, compact heat exchangers utilizing complex geometries. While correlations are specific to the geometries for which they were originally developed, numerical modeling, once validated, can be extended to non-conventional and more complicated geometries. Additionally, numerical modeling provides insight into the details of the flow field and transport phenomena. The present work focuses on the development of a purely theoretical, validated approach for modeling condensation heat transfer and the associated fluid flow characteristics in microchannels. For the purposes of this paper, we follow the widely accepted classification terminology of Kandlikar and Grande [5] which defines minichannels as channels having characteristic dimensions between 200 μm and 3 mm, and microchannels as those between 10 and 200 μm.

Existing approaches for modeling phase change phenomena under steady state conditions include the formulation proposed by

* Corresponding author. Address: Center for Environmental Energy Engineering (CEEE), 4164C Glenn L. Martin Hall, Department of Mechanical Engineering, University of Maryland, College Park, MD 20742, USA. Tel.: +1 301 405 5263; fax: +1 301 405 2025.
E-mail address: ohadi@umd.edu (M. Ohadi).

0017-9310/$ - see front matter © 2013 Elsevier Ltd. All rights reserved.
http://dx.doi.org/10.1016/j.ijheatmasstransfer.2013.05.044

Nomenclature

Bo	Bond number (–)
C	Courant number (–)
Ca	capillary number (–)
D	characteristic dimension (m)
E	energy per unit mass (J/kg)
f	friction factor (–)
F	force (N)
G	mass flux (kg/m^2 s)
h	heat transfer coefficient (W/m^2 K)
h_{LV}	latent heat (J/kg)
k	thermal conductivity (W/m K)
MAE	mean absolute error (%)
N	number of data points for calculating average
n_{phase}	number of phases
Nu	Nusselt number (–)
P	pressure (Pa)
q''	heat flux (W/m^2)
S_h	energy source term (kg/m s^3)
S_α	mass source term (kg/m^3 s)
t	time (s)
T	temperature (K)
V	velocity (m/s)
x	vapor quality (–)
X	Martinelli parameter (–)
Y	vertical axis in Cartesian coordinates
Z	horizontal axis in Cartesian coordinates

Greek symbols

α	volume/void fraction (–)
δ	thickness of thin liquid film (m)
ϕ	two-phase multiplier (–)
μ	dynamic viscosity (Pa s)
ρ	density (kg/m^3)

Subscripts and superscripts

A	acceleration
eff	effective
F	friction
i	denotes the ith phase
L	liquid
LO	liquid only
sat	saturation
TP	two-phase
V	vapor
VO	vapor only
$wall$	channel wall

Wang and Rose [6–8], wherein they reported a fundamental approach for laminar film condensation based on the Nusselt approximations, which was subsequently applied to study different minichannel geometries. Similarly, Wu et al. [9] reported a three-dimensional model for steady state annular condensation in rectangular microchannels.

While boiling heat transfer involves numerous, complex physical mechanisms, the physics governing evaporation, in addition to being simpler, also closely resembles that responsible for condensation heat transfer. From a modeling perspective, both these modes bear certain resemblances to the presently studied condensation heat transfer, and are therefore reviewed here. Heat transfer from thin films during evaporation comprises a meniscus region, an evaporating thin film region, and a nanoscale non-evaporating region. Wang et al. [10,11] utilized a Young–Laplace approach coupled with kinetic theory-based expressions for modeling thin film evaporation in microchannels. Subsequently, Mandel et al. [12] coupled the models of Wang et al. [8] and Xu and Carey [13] to obtain an improved formulation of the problem and therefore better accuracy. Modeling of similar problems using kinetic theory-based expressions in conjunction with commercial CFD codes was reported by Ranjan et al. [14] for thin film evaporation in capillary wicks and by Wang et al. [15] for an evaporating meniscus in an open V-microgroove.

All of the above studies were based on steady-state analysis. In other words, a solution of the governing equations yielded the profile of the liquid–vapor interface, based on which, the two-phase heat transfer performance was estimated. An alternative approach is to continuously track the transient liquid–vapor interface. This results in a highly accurate prediction of the interfacial area in the microchannel, which in turn influences the phase change mass flux and heat transfer. The method generally involves including mass and energy source terms in the multiphase flow model, and implementations of the same for film boiling problems have been reported by several groups. Juric and Tryggvason [16], Esmaeeli and Tryggvason [17,18], and Tryggvason et al. [19] implemented the front tracking model of Unverdi and Tryggvason [20], Son and Dhir [21] implemented the level set method of Sussman et al. [22], and Welch and Wilson [23] implemented the volume of fluid (VOF) method of Hirt and Nichols [24].

Zhang et al. [25] modeled condensation in a minichannel using the VOF model to govern the interface, and defined mass and energy source terms to model the phase change phenomena. A steady-state solution was obtained for the transient problem using a false transient method. The model was validated based on the liquid film thickness during Nusselt condensation on a vertical flat plate.

Mukherjee and Kandlikar [26] modeled the growth of a single bubble due to evaporation during flow boiling in a microchannel. This was a fundamental study that applied Fourier's law to estimate the heat flux at the liquid–vapor interface and determine the corresponding evaporation mass flux based on the latent heat. The level set method was implemented to govern the liquid–vapor interface. The results demonstrated the axial growth of a single bubble as it progressed through the channel and the same was qualitatively validated against the available experimental visualization data of Balasubramanian and Kandlikar [27].

Wu et al. [28] and Yang et al. [29] modeled flow boiling in conventional channels having a serpentine structure using the Eulerian and the VOF models, respectively. The phase change was modeled following the approach of Lee [30] which assumed a quasi-thermo equilibrium state at constant pressure, with the mass transfer being determined by the saturation temperature. Empirical coefficients were present in the expressions for the source terms and appropriate values for the same were recommended in order to maintain the interfacial temperature reasonably close to the saturation temperature, and to avoid divergence issues. The phase distribution in the channel was qualitatively compared with experimental visualization data.

Fang et al. [31] modeled flow boiling in a vapor–venting microchannel. The system was designed to locally vent the generated vapor phase into a separate secondary channel, thereby ensuring that the primary channel is predominantly occupied by the liquid phase. The interface was governed by the VOF model and their mass transfer formulation was similar to that of Yang et al. [29]. The effect of the porous membrane that performed the venting ac-

Table 1
Summary of select previous works relevant to the present study.

Authors	Heat transfer phenomena	Computational domain	Nature of model	Multiphase model	Validation of model
Zhang et al. [25]	Condensation	Minichannel (1.5 mm)	Theoretical	Volume of fluid	Quantitative: film thickness
Mukherjee and Kandlikar [26]	Evaporation of single bubble during flow boiling	Microchannel (100 μm)	Theoretical	Level set	Qualitative: transient bubble profiles
Wu et al. [28]	Flow boiling	Conventional channel (8 mm)	Theoretical	Eulerian	Qualitative: flow patterns
Yang et al. [29]	Flow boiling	Conventional channel (6 mm)	Theoretical	Volume of fluid	Qualitative: flow patterns
Fang et al. [31]	Flow boiling	Vapor venting microchannel (200 μm)	Theoretical	Volume of fluid	Qualitative: flow pattern; quantitative: liquid rise velocity in porous medium
Jeon et al. [32]	Condensation of a single bubble during subcooled flow boiling	Conventional channel (15 mm)	Theoretical and empirical expressions	Volume of fluid	Qualitative: transient bubble profile; quantitative: transient bubble volume
Zhuan and Wang [34]	Flow boiling	Microchannel (41, 48 μm)	Theoretical and empirical expressions	Volume of fluid	Quantitative: transient bubble diameter
Zhuan and Wang [35]	Flow boiling	Minichannel (768 μm)	Theoretical and empirical expressions	Volume of fluid	Quantitative: transient bubble diameter
Zhuan and Wang [36]	Subcooled flow boiling	Minichannel (200, 334 μm)	Theoretical and empirical expressions	Volume of fluid	Quantitative: void fraction, boiling curves
Zhuan and Wang [37]	Flow boiling	Minichannel (500 μm)	Theoretical and empirical expressions	Volume of fluid	Quantitative: bubble departure diameter, location and frequency, flow regime transition lines
Present work	Condensation	Microchannel (100 μm)	Theoretical	Volume of fluid	Qualitative: flow patterns; quantitative: frictional pressure drop and Nusselt number

tion was also considered and the associated flow patterns in these vapor–venting channels were compared with that obtained using non-venting channels. The former was reported to yield reductions in pressure drop, dry-out and flow instabilities.

Jeon et al. [32] studied the dynamics of a single condensing bubble during subcooled flow boiling in a conventional channel. The VOF method was used to govern the liquid–vapor interface. An empirical correlation derived by Kim and Park [33] was used to quantify the interfacial heat and mass transfer. The predictions of time-variant bubble volume were favorably compared with transient experimental measurements.

Wang and Zhuan [34] and Zhuan and Wang [35–37] modeled flow boiling in mini/microchannels having various cross-sectional geometries. The various regimes of the boiling process were modeled using known empirical expressions for the heat flux in each regime. The bubble characteristics, boiling curves and flow regime transition lines for certain flow patterns, primarily intermittent liquid–vapor flow patterns, were reported and compared against experimental data.

A summary of select previous works is reported in Table 1. The above review indicates that majority of the studies on transient numerical simulation of phase change phenomena have focused on boiling and evaporation heat transfer, and relatively fewer works have modeled transient condensation in microchannel geometries. Further, the use of empirical expressions integrated with the numerical governing equations appears to be a common way to model the physics of the phase change phenomena. While such studies are indeed valuable for certain simple geometries, their potential for application to any other geometry is limited by the availability of an empirical correlation for that particular geometry. Hence, it is essential to develop a purely theoretical and validated formulation that explicitly solves for the physics of the phenomena, which could be of use for the design of next-generation heat exchangers having complex, microscale geometries.

The present study proposes a purely theoretical, transient model for condensation heat transfer. The formulation is not restricted to a single bubble or a specific flow regime, but is targeted at the simulation of all condensation flow patterns. The model has been implemented for a relatively simple geometry, a single microchannel, for which well-established correlations are available in the literature. The predictions of two-phase pressure drop and Nusselt number have been compared against the correlational data. Additionally, condensation flow patterns have been simulated and compared against available experimental visualization data.

2. Governing equations

The present numerical formulation was implemented in a commercial CFD code, FLUENT version 6.3.26 (Ansys, Inc.). The numerical model for multiphase flow solved the equations for continuity, momentum conservation and energy conservation, as given by Eqs. (1)–(3), respectively.

$$\frac{\partial \rho}{\partial t} + \nabla \cdot (\rho \mathbf{V}) = 0 \tag{1}$$

$$\frac{\partial}{\partial t}(\rho \mathbf{V}) + \nabla \cdot (\rho \mathbf{V}\mathbf{V}) = -\nabla P + \nabla \cdot [\mu(\nabla \mathbf{V} + \nabla \mathbf{V}')] + \mathbf{F} \tag{2}$$

$$\frac{\partial}{\partial t}(\rho E) + \nabla \cdot [\mathbf{V}(\rho E + P)] = \nabla \cdot (k_{eff} \nabla T) + S_h \tag{3}$$

The multiphase flow was modeled by a finite volume method-based implementation of the VOF approach (Hirt and Nichols [24]). The surface tension forces were modeled following the continuum surface force (CSF) formulation of Brackbill et al. [38]. This approach models the pressure jump across the interface as a volume force that is included as a source term in the momentum equation. Additionally, the VOF model solves an equation for volume fraction, α, wherein for a multiphase system with k phases, Eq. (4) is solved

for $k-1$ phases, and the volume fraction of the excluded phase (termed the primary phase) is determined by the summation expression in Eq. (5).

$$\frac{\partial \rho_i \alpha_i}{\partial t} + \nabla \cdot (\rho_i \alpha_i \mathbf{V}_i) = S_{\alpha_i} \tag{4}$$

$$\sum_{i=1}^{n_{phase}} \alpha_i = 1 \tag{5}$$

The effective fluid properties such as density and viscosity were computed as the average property values of the two phases, weighted by their respective volume fractions. Interface reconstruction was performed using the explicit piecewise-linear interface construction (PLIC) scheme of Youngs [39]. A pressure-based solver with an unsteady first-order implicit formulation was utilized. A pressure-based coupled approach was found to yield improved stability as against a segregated approach for the pressure–velocity coupling, and hence this approach was used along with the PRESTO (pressure staggering option) scheme. Following the recommendations of Krishnan et al. [40], based on a detailed assessment on the performance of various numerical schemes for similar two-phase applications, a first-order upwind scheme for discretizing the momentum equation and a Green–Gauss node-based scheme for calculating the gradients of scalar variables were utilized.

Our modeling methodology aimed at avoiding the common assumption in several earlier works, which is to utilize a fixed interfacial profile between the liquid and vapor phase. This assumption is usually justified by considering the rate of mass transferred from one phase, say the vapor phase in the case of condensation, to exactly equal the mass flow rate of vapor entering the domain. However, such approaches are generally applicable only to certain flow regimes such as annular flow, where the profile of the interface is well established. Hence, it is believed that such models are not suitable for all flow regimes, and therefore developing a generic approach was one of the goals of the present study. In order to accomplish this, the phase change phenomenon was modeled in a manner that simultaneously considered the equations for fluid flow, heat transfer and the associated mass transfer. The use of an interface tracking algorithm allowed us to model both the gas and liquid phases, and hence interfacial motions resulting from the phase change process were successfully simulated. The latent heat associated with the phase change phenomena was modeled as an energy source and was represented by the term S_h in Eq. (3). Likewise, the source term accounting for mass transfer between the gas and liquid phases was given by the term S_{α_i} in Eq. (4). The heat flux associated with the phase change process in the interfacial region was estimated by applying Fourier's law (Eq. (6)). The same heat flux also relates the mass flux due to phase change and the latent heat (Eq. (7)).

$$(q'')_{\text{local,interface}} = -k_{eff} \times (\nabla T)_{\text{local,interface}} \tag{6}$$

$$(q'')_{\text{local,interface}} = (m'')_{\text{local,interface}} \times h_{LV} \tag{7}$$

Based on the above, the expressions for the mass source terms for the liquid and vapor phases were defined as given by Eqs. (8) and (9), respectively. The energy source term is given by Eq. (10).

$$(S_{\alpha_L})_{\text{local,interface}} = +\frac{(q'' \cdot \nabla \alpha)_{\text{local,interface}}}{h_{LV}} \tag{8}$$

$$S_{\alpha_V} = -S_{\alpha_L} = -\frac{(q'' \cdot \nabla \alpha)_{\text{local,interface}}}{h_{LV}} \tag{9}$$

$$S_h = +(S_{\alpha_L})_{\text{local,interface}} \times h_{LV} \tag{10}$$

It should be noted that the above expressions defining the mass and energy source terms were not part of the CFD code and were programmed into the numerical model by defining additional routines in C language as follows. The effective thermal conductivity, k_{eff}, was calculated as the average of thermal conductivities of the liquid and vapor phases, weighted by their respective volume fractions. The gradients of temperature and volume fraction were calculated using divergence theory, and were used to determine the three source terms given by Eqs. (8)–(10). The source terms were evaluated throughout the computational domain. However, their value is evaluated to equal zero everywhere, except in the vicinity of the liquid–vapor interface where the gradient of volume fraction is non-zero.

3. Numerical model

3.1. Computational domain

Since the present study was aimed at developing a numerical model and validating the predictions with known correlations for condensation phenomena, a relatively simple geometry was chosen for this purpose. A single microchannel was modeled as a two-dimensional geometry in the form of a rectangular domain, a schematic of which is presented in Fig. 1.

The microchannel had a characteristic dimension, D, equaling 100 μm and a length of 0.03 m. A velocity boundary condition was specified at the channel inlet for the superheated vapor phase, and a pressure-based boundary condition was specified at the channel outlet. A constant heat flux was specified at the channel walls. In order to simplify the analysis, the solid microchannel wall was not modeled, and therefore the effects of wall conduction were not accounted for in the present study.

The entire domain was discretized with a homogeneous structured grid consisting of quadrilateral elements with a size of 2 μm (D/50). The use of a locally refined grid near the channel wall was considered since this could potentially assist in capturing thin liquid films during certain flow conditions such as that involving slug and annular flow patterns. While several previous studies on modeling of two-phase flow phenomena have used non-uniform grids [41–44], certain others have preferred to use uniform element sizes throughout the computational domain [26,35–37,40,45–52]. One of the reasons for the same is to maintain a constant resolution of the liquid–vapor interface throughout the computational domain. Further, this strategy does not facilitate capturing the spatially fine flow features that occur in regions away from the channel wall. For these reasons, a uniform grid was utilized in the present study.

3.2. Simulation conditions

1,1,1,2-Tetrafluoroethane, more commonly referred to as R-134a or HFC-134a was used as the working fluid, whose thermo-physical properties were obtained from the program REFPROP 9.0 (Lemmon et al. [53]) at the saturation temperature corresponding to a system pressure of 1 MPa. The pressure drop across the channel was relatively small compared to the system pressure for the channel length under consideration in the present work. Hence, the variation in thermo-physical properties across the channel length was neglected. The constant values, taken at the saturation temperature corresponding to 1 MPa system pressure are summarized in Table 2. The incoming vapor was superheated by 10 K, and the magnitude of negative heat flux (heat removal during condensation) applied to the channel wall ranged between 200 and 800 kW/m^2. The vapor mass flux at the inlet ranged from 246 to 615 kg/m^2 s.

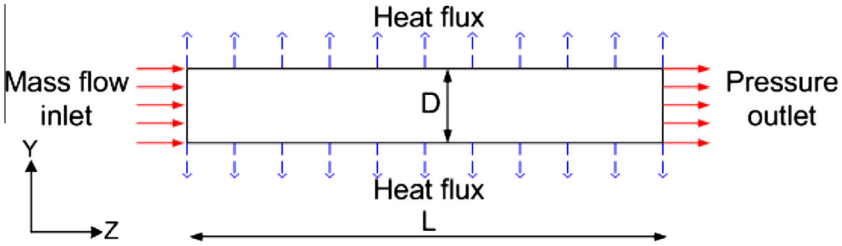

Fig. 1. Schematic of computational domain.

Table 2
Thermo-physical properties of R134a at system pressure of 1 MPa corresponding to saturation temperature of 312.54 K [53].

Property	Liquid phase	Gas phase	Two-phase
Density (kg/m^3)	1149.3	49.22	–
Dynamic viscosity (μPa s)	162.7	12.34	–
Thermal conductivity (W/m K)	0.0749	0.0154	–
Enthalpy (kJ/kg)	255.50	419.16	–
Specific heat capacity (J/kg K)	1494.8	1139.1	–
Latent heat (kJ/kg)	–	–	163.66
Surface tension (N/m)	–	–	0.0062

The Bond number criterion of Brauner and Moalem-Maron [54], $Bo < (2\pi)^2$, was used to verify that at the present length scale, the surface tension forces were indeed dominant over gravitational forces and hence the latter could be neglected. Additionally, as noted in Section 4.4, gravitational head-based pressure drops were not present.

Wang et al. [15] reported that Marangoni convection currents do arise during phase change heat transfer in similar microscale geometries due to non-uniform interfacial temperatures. However, they demonstrated that the effect of the same on heat transfer was relatively negligible. Following their analysis and the assumptions made in other modeling studies (Mukherjee and Kandlikar [26], Fang et al. [31]), the effects of Marangoni convection have been neglected in the present simulations.

3.3. Surface wettability

The surface wettability can influence the fluid flow and heat transfer characteristics during condensation in microchannels. The experimental study of Fang et al. [55] demonstrated that channels with hydrophobic surfaces yield better thermal performances as compared to those with hydrophilic surfaces. The same was attributed to the differences in flow patterns and hence the heat transfer mechanisms. The present VOF formulation can account for surface wetting by altering the interface normal in the near-wall cells based on the specified value of contact angle, and such an approach has been followed in several works [43–45,48–50]. However, various deficiencies in the above approach were identified by Santos and Kawaji [49], Ganapathy et al. [50], and Fang et al. [56], which include the inability to account for contact angle hysteresis, the lack calculation of dynamic contact angles, the lack of modeling of contact line slip, and use of a constant pre-determined value of contact angle. Addressing these deficiencies is an active area of research and numerous techniques for the same have been suggested in the literature (Fang et al. [56], Renardy et al. [57], and Thomas et al. [58]). However, the inclusion of these approaches significantly adds to the complexity of the present problem and hence, the effects of surface wettability were not considered in the present simulations. It is recommended that future efforts account for the surface wettability effects and overcome the corresponding deficiencies otherwise.

3.4. Transient solver settings

The transient solution for the governing equations was obtained using an explicit scheme for which the Courant number was used to adopt a variable time-stepping strategy. The Courant number, C, is a non-dimensional quantity defined by Eq. (11) as the ratio of the time step size used by the transient solver, Δt, to the characteristic time required for a fluid element to transit a control volume. The latter is calculated based on the cell volume and the sum of the outgoing fluxes, thereby yielding the duration it takes for fluid to empty out of any given cell. The smallest time associated with all the cells in the control volume is used to determine the appropriate size of the time step to be chosen in order to remain within the specified value of Courant number.

$$C = \frac{\Delta t}{\Delta x_{cell}/V_{fluid}} \tag{11}$$

An exceedingly low value of Courant number corresponds to a very small time-step size and is associated with a high computational cost. However, this case yields high predictive accuracy with respect to being able to capture all physical flow features. An unphysical high Courant number may result in poor simulation of the transient flow features and possibly divergence of the solution.

In the present study, the Courant number for solving the volume fraction equation (Eq. (4)) was restricted to 0.25, while that for the remaining transport equations (Eqs. (1)–(3)) was restricted to a higher value of 5. With these settings multiple flow patterns were captured which was considered an indication of the appropriateness of the above solver settings (Krishnan et al. [40]). Similar values have been reported by Liu and Wang [42], Qian and Lawal [45] and Gupta et al. [48].

4. Results and discussion

4.1. Grid independence

Domain discretization was performed at a coarse level having an element size of 20 μm and was sequentially refined to a fine level having an element size of 2 μm. The average wall temperature was monitored over the condensing region of the computational domain for these levels of domain discretization. The results of the grid independence analysis are reported in Fig. 2, for an inlet vapor mass flux of 492.2 kg/m^2 s. The average deviation in wall temperature between the results for the 5 and 2 μm, for the four levels of heat flux reported in Fig. 2, was only 0.79%. While our initial conclusion was that 5 μm elements could be satisfactorily utilized, the ability of the discretized domain to capture thin liquid films typically associated with microscale flows was further assessed using the methodology proposed by Gupta et al. [48]. The capillary number ranged from 0.13 to 0.32 in the present study. Correlations to estimate the thickness of the liquid film as a function of capillary number have been reported in the literature,

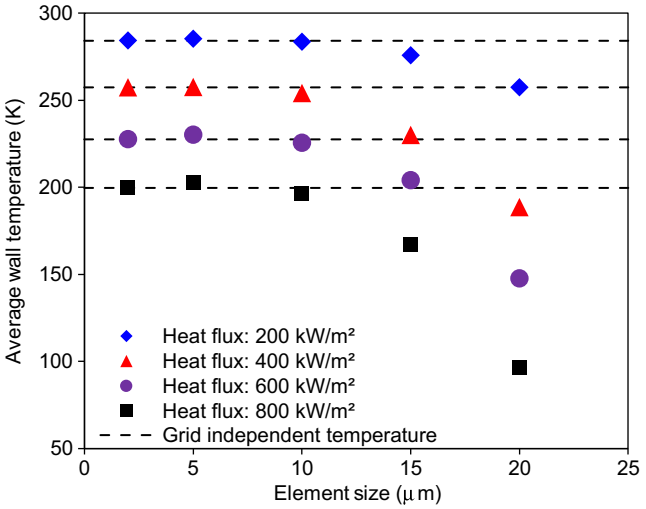

Fig. 2. Analysis of average wall temperature to determine grid independence.

including Eqs. (12) and (13), by Bretherton [59] and Aussillous and Quere [60], respectively.

$$\frac{2\delta}{D} = 1.34Ca^{2/3} \tag{12}$$

$$\frac{2\delta}{D} = \frac{1.34Ca^{2/3}}{1 + 2.5(1.34Ca^{2/3})} \tag{13}$$

Gupta et al. [48] stated that these expressions could be used to estimate the thickness of typical liquid films and thereby ensure that the computational domain is resolved such that sufficient computational cells are present across the above-obtained value of film thickness. Eq. (13) [60] was found to yield a more conservative prediction and therefore, was used in the present study. Characteristic results of the same for an inlet vapor mass flux of 492.2 kg/m^2 s and wall heat flux of 400 kW/m^2 are reported in Table 3. As can be seen, a 5 μm element size yields less than five mesh elements across a typical liquid film and therefore was concluded to be insufficient. An element size of 2 μm corresponds to a thin film resolution factor of 12 and so was employed for the remainder of the study. It is worth noting that this selection alone resulted in a six-fold increase in the number of computational cells and therefore significantly longer simulation times.

4.2. Analysis of condensation flow regimes

Gas-liquid two-phase flow at the microscale is associated with several flow patterns that have been visualized in numerous past experimental works [61–67]. In the present work, various condensation flow regimes were observed at various locations along the channel length at different operating conditions. The predicted flow regimes were compared with experimental visualization data from the literature for condensing flows and are reported in Fig. 3. It is noted that this comparison is qualitative in nature and that the channel geometry and operating conditions used to obtain the present simulation-based results do not correspond to the conditions under which the experimental data was obtained. The condensation flow regimes have been classified into three major categories as described below.

4.2.1. Annular flow

Annular flow is typically characterized by a core of vapor flowing through the center of the channel surrounded by a thin film of liquid along the channel wall. Smooth and wavy annular flow regimes are reported in Fig. 3a and b, respectively. Both have been compared against the visualization data of Kim et al. [67], and a good resemblance was obtained. While smooth annular flow comprises a relatively straight/flat interface profile, the wavy annular flow regime is characterized by a wavy interfacial profile comprising crests and troughs. Coleman and Garimella [61] noted that the liquid and vapor phases can move at different velocities, and when this is a dominant occurrence, the resulting shear forces at the interface lead to the formation of waves. Fang et al. [66] used an optical interference technique to obtain the topology of the interface and the above-described wave-like instabilities were reported to have amplitude on the order of a few microns. Mist/droplet flow is reported in Fig. 3 c and favorably compared against the experimental data of Wu and Cheng [62]. This regime is characterized by numerous tiny droplets of liquid entrained in the bulk vapor phase.

4.2.2. Transitional flow

Transitional flow patterns are comprised of four sub-types. Smooth discrete and wavy discrete flows are reported in Fig. 3c and d, and have been compared against the experimental visualization data of Hu and Chao [63] and Coleman and Garimella [61], respectively. Both of these are very similar to the previously discussed annular flow regimes, except for the presence of numerous liquid droplets entrained in the central vapor core. The dispersed/churn flow regime was characterized by a seemingly random distribution of the unstable vapor phase surrounded by the liquid phase. Fig. 3f compares the predicted flow pattern against the experimental visualization of Coleman and Garimella [61], who classified it as disperse wavy flow with a high intensity of secondary waves. They attributed the occurrence of this regime to an increase in the intensity of the waves discussed above, which results in the surface of the wavy interface contacting the channel wall, causing a dispersion of the waves. At higher wave intensities, multiple waves may be superimposed on each other, making the liquid–vapor interface indistinguishable.

4.2.3. Intermittent flow

Intermittent flow patterns are characterized by alternating regions composed of predominantly either the liquid or vapor phase only. Slug flow and bubbly flow are reported by Fig. 3g and h, respectively, and both were compared with the experimental visu-

Table 3
Characteristic results from grid independence studies for inlet vapor mass flux of 492.2 kg/m^2 s and wall heat flux of 400 kW/m^2.

Element size (μm)	Computational cells (–)	Average wall temperature (K)	Discrepancy[a] (%)	Resolution of thin film[b] (–)
2	750,000	257.37	–	12.0
5	120,000	257.55	0.07	4.8
10	30,000	254.07	1.28	2.4
15	13,333	230.00	10.63	1.6
20	7500	188.57	26.73	1.2

[a] Discrepancy between current case and 2 μm case.
[b] Calculated as the ratio of least thickness of thin liquid film in current range of operating conditions (as estimated by Aussillous and Quere [60]) to the element size.

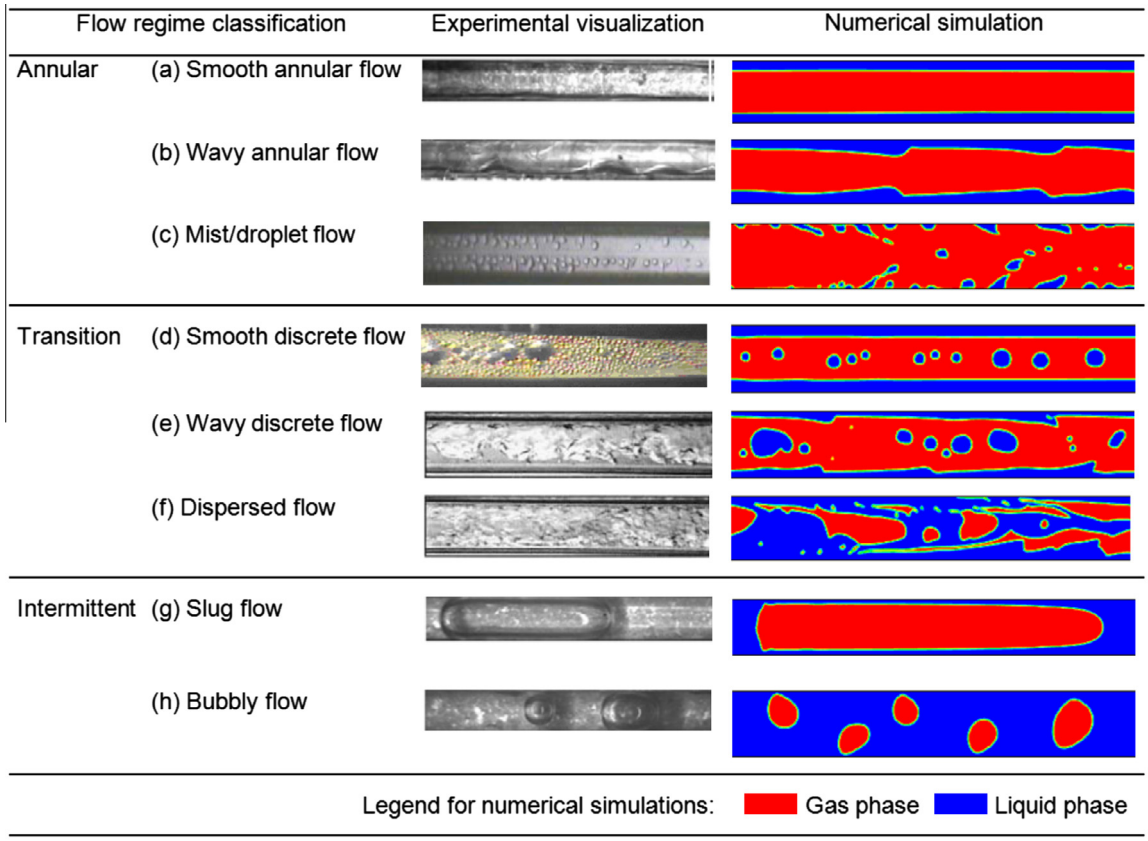

Fig. 3. Comparison of numerically predicted condensation flow regimes in the microchannel with experimental visualization data in the literature (a) smooth annular flow; (b) wavy annular flow; (c) mist/droplet flow; (d) smooth discrete flow; (e) wavy discrete flow; (f) dispersed flow; (g) slug flow; (h) bubbly flow. Experimental visualization images (a,b,g,h) were reprinted from Kim and Mudawar [67] (Copyright 2012, with permission from Elsevier); (c) reprinted from Wu and Cheng [62] (Copyright 2005, with permission from Elsevier); (d) Hu and Chao [63] (Copyright 2007, with permission from Elsevier); (e,f) Coleman and Garimella [61] (Copyright 2003, with permission from Elsevier).

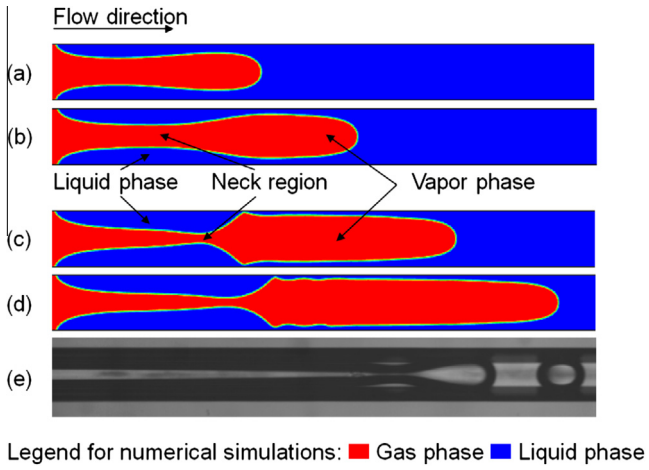

Fig. 4. (a–d) Numerically predicted contours of vapor void fraction of various stages of bubble growth during injection flow; (e) experimental visualization image from Wu et al. [64] (© IOP Publishing. Reproduced by permission of IOP Publishing. All rights reserved).

alization data of Kim et al. [67]. Slug flow is characterized by alternating regions of elongated vapor bubbles and liquid slugs. The vapor bubbles are typically longer than the channel width and are separated from the channel wall by a thin film of liquid. On the other hand, bubbly flow is characterized by numerous vapor bubbles present in the bulk liquid phase wherein the bubble lengths are typically only a fraction of the channel width.

The mechanism of bubble formation and detachment which subsequently results in the formation of vapor bubbles and liquid slugs is termed as injection flow. The results reported in Fig. 4a–d from the numerical simulations and those in Fig. 4e from Wu et al. [64] indicate the various stages of formation of a neck region

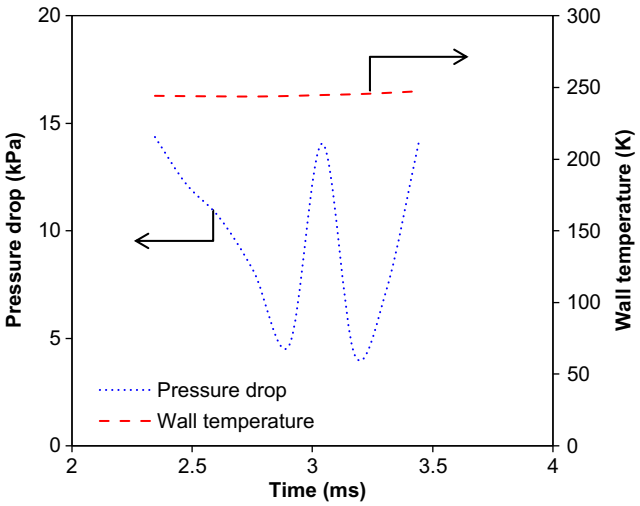

Fig. 5. Transient variation of pressure drop and wall temperature in microchannel for heat flux of 600 kW/m^2 and inlet vapor mass flux of 492 kg/m^2 s (average pressure is 9.98 kPa and average temperature is 244.89 K).

between the emerging vapor bubble and the upstream bulk vapor phase, leading to detachment of the bubble.

The above results indicate that the numerical model proposed in the present work has a high qualitative accuracy with respect to the simulation of condensation flow patterns. A more detailed effort to analyze quantitative flow regime transition criteria is underway and will be reported in the future. Quantitative validation of the numerical model with respect to two-phase frictional pressure drop and two-phase Nusselt number is reported subsequently.

4.3. Data reduction: pressure drop and temperature

The pressure drop in the channel was observed to fluctuate in a periodic manner, and the average value was obtained by determining the mean pressure drop over multiple cycles for a given operating condition. The average wall temperature was observed to be relatively constant with respect to time. Fig. 5 reports the transient variation of pressure drop and surface temperature for a typical case of condensation heat transfer with a heat flux of 600 kW/m^2 and inlet vapor mass flux of 492 kg/m^2 s. The fluctuations in pressure drop were attributed to the phenomena occurring within the computational domain pertaining to the flow patterns reported in Fig. 3. These include the formation of liquid droplets in mist, smooth discrete and wavy discrete flow patterns (Fig. 3c–e), and the formation of intermittent vapor bubbles in slug and bubbly flow patterns (Fig. 3g and h). Similar pressure fluctuations during phase change heat transfer, albeit for boiling mode, were reported by Zhang et al. [68] and Fang et al. [31]. However, the observed frequencies are dependent on the time step size and sampling rate and hence, are not expected to have any physical significance.

4.4. Two-phase pressure drop

The two-phase pressure drop predicted by the numerical model was a summation of the components due to friction and acceleration effects. As per the assumption stated in Section 3.2, gravitational pressure losses were not considered in the present simulations. The acceleration pressure drop was estimated from Eq. (14) and subtracted from the total two-phase pressure drop predicted by the numerical model to yield the frictional pressure drop.

$$\left(-\frac{dP}{dZ}\right)_{TP,A} = G^2 \frac{d}{dZ}\left[\left(\frac{x^2}{\alpha\rho_V}\right) + \left(\frac{(1-x)^2}{(1-\alpha)\rho_L}\right)\right] \tag{14}$$

An analysis of the two-phase frictional pressure drop was performed using the separated flow approach, which involves the use of two-phase multipliers. Eq. (15) defines ϕ_L^2 and ϕ_V^2 which pertain to cases when either pure liquid or pure vapor flows in the channel at a mass flux of $G(1-x)$ or Gx, respectively. An alternative definition for the two-phase multiplier is provided by Eq. (16). Here ϕ_{LO}^2 and ϕ_{VO}^2 pertain to the cases when all the mixture in the channel is either only liquid or only vapor, at a mass flux of G.

$$\left(-\frac{dP}{dZ}\right)_{TP,F} = \phi_L^2 \cdot \left(-\frac{dP}{dZ}\right)_{L,F} = \phi_V^2 \cdot \left(-\frac{dP}{dZ}\right)_{V,F} \tag{15}$$

$$\left(-\frac{dP}{dZ}\right)_{TP,F} = \phi_{LO}^2 \cdot \left(-\frac{dP}{dZ}\right)_{LO,F} = \phi_{VO}^2 \cdot \left(-\frac{dP}{dZ}\right)_{VO,F} \tag{16}$$

The definitions of the corresponding single-phase pressure drops for the above cases are given by Eqs. (17) and (18) for the liquid phase, and by Eqs. (19) and (20) for vapor phase, respectively. The Martinelli parameter, X, is the ratio of the single-phase pressure drop in the liquid phase to that in the gas phase (Eq. (21)).

$$\left(-\frac{dP}{dZ}\right)_{L,F} = \frac{f_L[G(1-x)]^2}{2\rho_L D_h} \tag{17}$$

$$\left(-\frac{dP}{dZ}\right)_{LO,F} = \frac{f_{LO}G^2}{2\rho_L D_h} \tag{18}$$

$$\left(-\frac{dP}{dZ}\right)_{V,F} = \frac{f_V[Gx]^2}{2\rho_V D_h} \tag{19}$$

$$\left(-\frac{dP}{dZ}\right)_{VO,F} = \frac{f_{VO}G^2}{2\rho_V D_h} \tag{20}$$

$$X^2 = \left(-\frac{dP}{dZ}\right)_{L,F} \Big/ \left(-\frac{dP}{dZ}\right)_{V,F} = \phi_V^2/\phi_L^2 \tag{21}$$

The numerically predicted pressure drop was used to calculate the non-dimensional two-phase multiplier. The vapor quality in the present study was estimated from the numerically predicted void fraction, in conjunction with the homogeneous flow model expression given by Eq. (22).

$$\alpha = \left[1 + \left(\frac{1-x}{x}\right)\cdot\left(\frac{\rho_V}{\rho_L}\right)\right]^{-1} \tag{22}$$

The two-phase viscosity, which is a function of the vapor quality, was calculated using the correlation of McAdams et al. [69], given by Eq. (23). The mixture density was determined from Eq. (24). μ_{TP} and ρ_{TP} were used to determine the total mass flux of the two-phase flow.

$$\mu_{TP} = \left(\frac{x}{\mu_V} + \frac{1-x}{\mu_L}\right)^{-1} \tag{23}$$

$$\rho_{TP} = \left(\frac{x}{\rho_V} + \frac{1-x}{\rho_L}\right)^{-1} \tag{24}$$

The variation of the two-phase multiplier, ϕ_L^2, with the Martinelli parameter, X, as obtained from the present numerical simulations and available empirical correlations in the literature, is reported in Fig. 6. Additionally, a parity plot comparing the numerical and empirical values of ϕ_L^2, for various values of X, is reported in Fig. 7. The mean absolute error (MAE) was estimated from Eq. (25) and the values are summarized in Table 4 along with a brief description of the expressions.

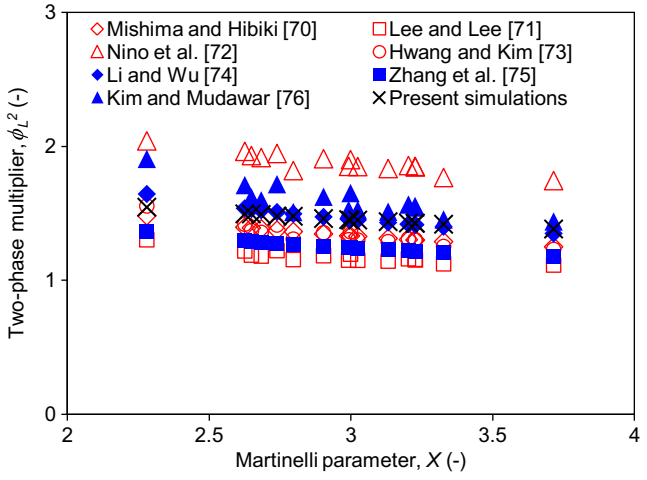

Fig. 6. Variation of empirical and numerically predicted two-phase multiplier, ϕ_L^2, with Martinelli parameter, X.

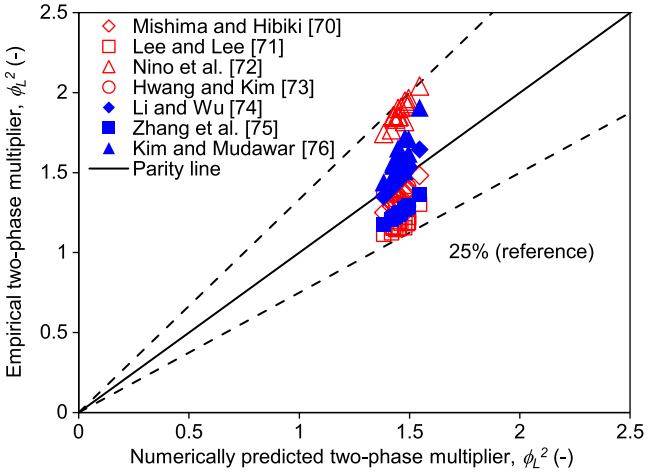

Fig. 7. Validation of two-phase frictional pressure drop by comparing numerically predicted two-phase multiplier, ϕ_L^2, with empirical correlations. All predictions are within an MAE of 25%.

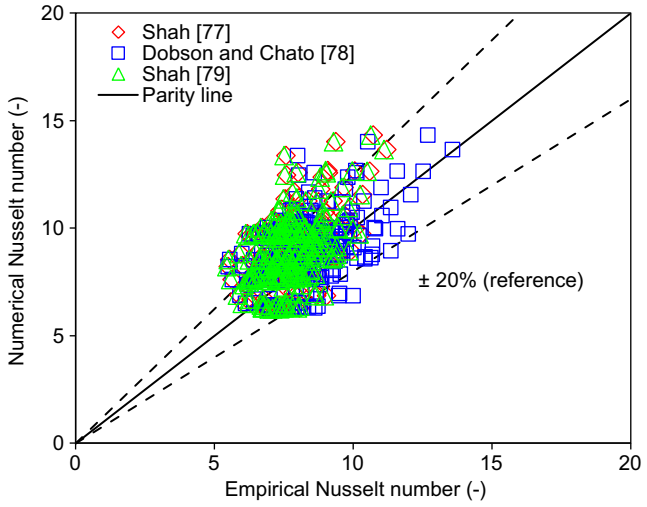

Fig. 8. Validation of numerically predicted two-phase Nusselt number by comparison with empirical correlations.

Table 4
Comparison of numerically predicted two-phase frictional pressure drop with empirical correlations.

Authors	Characteristic dimensions	Working fluid (s)	MAE (%)
Mishima and Hibiki [70]	1.05–4.08 mm	Air/water	8.5
Lee and Lee [71]	0.78–6.67 mm	Air/water	24.9
Nino et al. [72]	1.02–1.54 mm	Air/water, R134a, R410A	21.9
Hwang and Kim [73]	0.244–0.792 mm	R134a	9.6
Li and Wu [74]	0.148–3.25 mm	769 data points obtained from the literature involving 12 working fluids (55% of the data based on R134a)	1.5
Zhang et al. [75]	0.007–6.25 mm	2201 data points obtained from the literature involving 10 working fluids	16.5
Kim and Mudawar [76]	0.0695–6.22 mm	7115 data points obtained from the literature involving 17 working fluids	8.1

$$(\mathrm{MAE})_{\phi_L^2} = \frac{1}{N}\sum_{N}\frac{\left|(\phi_L^2)_{numerical} - (\phi_L^2)_{correlation}\right|}{(\phi_L^2)_{correlation}} \times 100\% \tag{25}$$

A good agreement, with an MAE less than 25%, was obtained with the correlations by Mishima and Hibiki [70], Lee and Lee [71], Nino et al. [72], Hwang and Kim [73], Li and Wu [74], Zhang et al. [75] and Kim and Mudawar [76]. Particularly, it is worth mentioning the recent expression by Kim and Mudawar [76] which was proposed as a universal approach for two-phase frictional pressure drop. The same was developed based on a large database comprising 7115 experimental data points from the literature for adiabatic and condensing flows largely in minichannels and microchannels (69.5 μm to 6.22 mm) involving 17 working fluids. The present simulations yielded an MAE of 8.1% with the above-described universal approach.

Table 5
Comparison of numerically predicted two-phase Nusselt number with empirical correlations.

Author(s)	Characteristic dimension	Working fluids	MAE (%)
Shah [77]	7.4–40 mm	473 data points obtained from the literature involving 10 working fluids	19.1
Dobson and Chato [78]	3.14–7.04 mm	R12, R22, R134a, R32/R125	16.6
Shah [79]	2–49 mm	1189 data points obtained from the literature involving 22 working fluids	20.2

All of the above were considered indicative of the reasonably good predictive accuracy of the current numerical model with respect to pressure drop.

4.5. Two-phase Nusselt number

The two-phase heat transfer coefficient was estimated from Eq. (26) and subsequently used to calculate the Nusselt number from Eq. (27). The calculated Nusselt number was compared against the empirical correlations listed in Table 5 by Shah [77], Dobson and Chato [78], and Shah [79] where the MAE values were estimated from Eq. (28).

$$h_{TP} = \frac{q''}{T_{sat} - T_{wall}} \tag{26}$$

$$Nu_{TP} = \frac{h_{TP}D}{k_L} \tag{27}$$

$$(\mathrm{MAE})_{Nu_{TP}} = \frac{1}{N}\sum_{N}\frac{\left|(Nu_{TP})_{numerical} - (Nu_{TP})_{correlation}\right|}{(Nu_{TP})_{correlation}} \times 100\% \tag{28}$$

The results are reported in Fig. 8, and MAE values of 19.1%, 16.6% and 20.2% were obtained with the correlations of Shah [77], Dobson and Chato [78], and Shah [79], respectively. While these expressions do have their own accuracy when compared to various sources of experimental data in the literature, the presently obtained values of MAE were considered to be indicative of a reasonably acceptable level of predictive accuracy of the current numerical formulation with respect to heat transfer characteristics during condensation

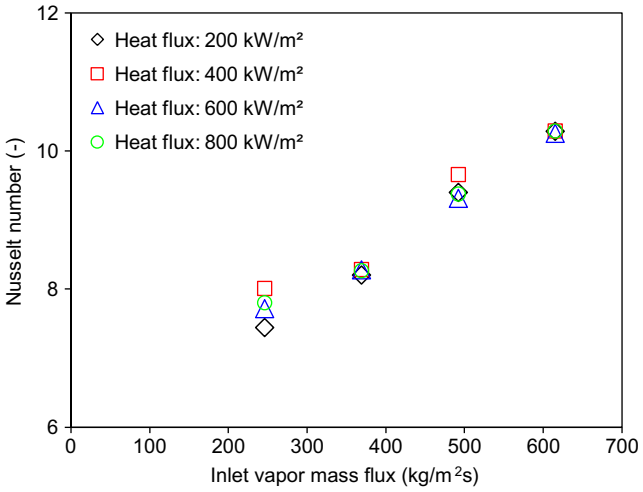

Fig. 9. Variation of two-phase Nusselt number with inlet vapor mass flux for different levels of wall heat flux.

in microchannels. Additionally, it is worth noting that the expressions listed in Table 5 were predominantly developed for conventional channel sizes only. Given this fact, it is interesting to observe the good predictive accuracy of these expressions for the present 100 μm channel. However, numerous recent works have found the same expressions to be suitable for mini/microchannel applications. The correlation by Shah [77] compared well against the experimental data of Shin and Kim [80] for condensation in a 690 μm channel. Likewise, Derby et al. [81] studied square, triangular and semi-circular cross-sections in a 1 mm channel and reported that their experimental condensation data for all cross-sections were in best agreement with the expressions by Shah [77] and Shah [79], as compared to certain available alternatives. Kim and Mudawar [82] have demonstrated the effectiveness of the correlations by Shah [77] and Dobson and Chato [78] in predicting their experimental data for condensation in a 1 mm channel. The current results serve as additional verification of the suitability of the presently tested conventional channel correlations for micro-level length scales as well.

The variation of Nusselt number with inlet vapor mass flux for various levels of wall heat flux is reported in Fig. 9. The trend indicating an increase in Nusselt number with increasing mass flux can be attributed to the relative dominance of certain flow regimes over a larger portion of the channel length at different mass flux levels. Additionally, the Nusselt number curves have a steep positive slope with respect to increasing mass fluxes, which is a characteristic feature of condensation associated with high levels of vapor quality (Wang et al. [83]), as was the case in the present study, which considered superheated vapor at the inlet.

5. Conclusions

The current work proposed a purely theoretical modeling approach for the simulation of condensation heat transfer in microchannels. The developed model was based on the volume of fluid method for governing the hydrodynamics of the liquid and vapor phases. Source terms were defined in the governing equations for volume fraction and energy in order to account for the heat and mass transfer due to condensation. All simulations were based on a channel with characteristic dimension of 100 μm and R134a as the working fluid. The numerically simulated condensation flow regimes were qualitatively compared against available experimental visualization data, and a favorable agreement was obtained. Further, the quantitative predictive accuracy of the proposed model was assessed by comparing the two-phase frictional pressure drop and two-phase Nusselt number against numerous empirical correlations in the literature, and a reasonably good agreement was obtained. The two-phase pressure drop was predicted within an MAE of 8.1% with a recent universal predictive approach reported in the literature. The Nusselt number was predicted within an MAE of 16.6% with an empirical correlation available in the literature. Based on the validation studies performed in the present work, the proposed numerical formulation was concluded to have a reasonable level of predictive accuracy that supports its potential application towards the simulation of condensation heat transfer in more complex microscale geometries as a design tool for the development of next-generation, ultra-compact, phase-change heat exchangers.

Acknowledgements

The authors gratefully acknowledge the financial support provided by GASCO and ADGAS companies of ADNOC Group companies, Abu Dhabi, United Arab Emirates. The authors are also grateful to members of the Research and Development Gas Sub-Committee of ADNOC Group for their close technical interaction and support.

References

[1] D.B. Tuckerman, R.F.W. Pease, High-performance heat sinking for VLSI, IEEE Electron Device Lett. 2 (5) (1981) 126–129.
[2] C.B. Sobhan, S.V. Garimella, A comparative analysis of studies on heat transfer and fluid flow in microchannels, Microscale Thermophys. Eng. 5 (2001) 293–311.
[3] M. Ohadi, K. Choo, S. Dessiatoun, E. Cetegen, Next Generation Microchannel Heat Exchangers, Springer, New York, 2013. pp. 33–65.
[4] Y.J. Kim, Y.K. Joshi, A.G. Fedorov, An absorption based miniature heat pump system for electronics cooling, Int. J. Refrig. 31 (2008) 23–33.
[5] S.G. Kandlikar, W.J. Grande, Evolution of microchannel flow passages–thermohydraulic performance and fabrication technology, Heat Transfer Eng. 24 (1) (2003) 3–17.
[6] H.S. Wang, J.R. Rose, A theory of film condensation in horizontal noncircular section microchannels, J. Heat Transfer 127 (2005) 1096–1104.
[7] H.S. Wang, J.R. Rose, Film condensation in horizontal microchannels: effect of channel shape, Int. J. Therm. Sci. 45 (2006) 1205–1212.
[8] H.S. Wang, J.R. Rose, Theory of heat transfer during condensation in microchannels, Int. J. Heat Mass Transfer 54 (2011) 2525–2534.
[9] J. Wu, Y. Chen, M. Shi, P. Fu, G.P. Peterson, Three-dimensional numerical simulation for annular condensation in rectangular microchannels, Nanoscale Microscale Thermophys. Eng. 13 (2009) 13–29.
[10] H. Wang, S.V. Garimella, J.Y. Murthy, Characteristics of an evaporating thin film in a microchannel, Int. J. Heat Mass Transfer 50 (2007) 3933–3942.
[11] H. Wang, S.V. Garimella, J.Y. Murthy, An analytical solution for the total heat transfer in the thin-film region of an evaporating meniscus, Int. J. Heat Mass Transfer 51 (2007) 6317–6322.
[12] R.K. Mandel, M.M. Ohadi, A. Shooshtari, S.V. Dessiatoun, Thin film evaporation on microstructured surfaces–application to cooling high heat flux electronics, in: Proceedings of 27th Annual IEEE Semiconductor Thermal Measurement and Management Symposium (SEMI-THERM), 2011, pp. 138–145.
[13] X. Xu, P. Carey, Film evaporation from a micro-grooved surface-an approximate heat transfer model and its comparison with experimental data, J. Thermophys. 4 (1990) 512–520.
[14] R. Ranjan, J.Y. Murthy, S.V. Garimella, A microscale model for thin-film evaporation in capillary wick structures, Int. J. Heat Mass Transfer 54 (2011) 169–179.
[15] H. Wang, Z. Pan, S.V. Garimella, Numerical investigation of heat and mass transfer from an evaporating meniscus in a heated open groove, Int. J. Heat Mass Transfer 54 (2011) 3015–3023.
[16] D. Juric, G. Tryggvason, Computations of boiling flows, Int. J. Multiphase Flow 24 (1998) 387–410.
[17] A. Esmaeeli, G. Tryggvason, Computations of film boiling. Part I: Numerical method, Int. J. Heat Mass Transfer 47 (2004) 5451–5461.
[18] A. Esmaeeli, G. Tryggvason, Computations of film boiling. Part II: Multi-mode film boiling, Int. J. Heat Mass Transfer 47 (2004) 5463–5476.
[19] G. Tryggvason, A. Esmaeeli, N. Al-Rawahi, Direct numerical simulations of flows with phase change, Comput. Struct. 83 (2005) 445–453.
[20] S.O. Unverdi, G. Tryggvason, A front-tracking method for viscous, incompressible, multi-fluid flows, J. Comput. Phys. 100 (1992) 25–37.
[21] S. Son, V.K. Dhir, Numerical simulation of film boiling near critical pressures with a level set method, J. Heat Transfer 120 (1998) 183–192.
[22] M. Sussman, P. Smereka, S. Osher, A level set approach for computing solutions to incompressible two-phase flow, J. Comput. Phys. 114 (1994) 146–159.

[23] S.W.J. Welch, J. Wilson, A volume of fluid based method for fluid flows with phase change, J. Comput. Phys. 160 (2000) 662–682.
[24] C.W. Hirt, B.D. Nichols, Volume of fluid (VOF) method for the dynamics of free boundaries, J. Comput. Phys. 39 (1981) 201–225.
[25] Y. Zhang, A. Faghri, M.B. Shafii, Capillary blocking in forced convective condensation in horizontal miniature channels, J. Heat Transfer 123 (2001) 501–511.
[26] A. Mukherjee, S.G. Kandlikar, Numerical simulation of growth of a vapor bubble during flow boiling of water in a microchannel, Microfluid Nanofluid 1 (2005) 137–145.
[27] P. Balasubramanian, S.G. Kandlikar, An experimental study of flow patterns, pressure drop and flow instabilities in parallel rectangular minichannels, in: Proceedings of the 2nd International Conference on Microchannels and Minichannels, Rochester, New York, 2004, pp. 475–481.
[28] H.L. Wu, X.F. Peng, P. Ye, Y.E. Gong, Simulation of refrigerant flow boiling in serpentine tubes, Int. J. Heat Mass Transfer 50 (2007) 1186–1195.
[29] Z. Yang, X.F. Peng, P. Ye, Numerical and experimental investigation of two phase flow during boiling in a coiled tube, Int. J. Heat Mass Transfer 51 (2008) 1003–1016.
[30] W.H. Lee, A pressure iteration scheme for two-phase flow modeling, in: T.N. Veziroglu (Ed.), Multiphase Transport Fundamentals, Reactor Safety, Applications, 1, Hemisphere Publishing, Washington, DC, 1980.
[31] C. Fang, M. David, A. Rogacs, K. Goodson, Volume of fluid simulation of boiling two-phase flow in a vapor venting microchannel, Front. Heat Mass Transfer 1 (2010) 013002.
[32] S.S. Jeon, S.J. Kim, G.C. Park, Numerical study of condensing bubble in subcooled boiling flow using volume of fluid model, Chem. Eng. Sci. 66 (2011) 5899–5909.
[33] S.J. Kim, G.C. Park, Interfacial heat transfer of condensing bubble in subcooled boiling flow at low pressure, Int. J. Heat Mass Transfer 54 (2011) 2962–2974.
[34] W. Wang, R. Zhuan, Numerical simulation of micro scale flowing and boiling, Front. Energy Power Eng. Chin. 3 (4) (2008) 396–401.
[35] R. Zhuan, W. Wang, Simulation on nucleate boiling in micro-channel, Int. J. Heat Mass Transfer 53 (2010) 502–512.
[36] R. Zhuan, W. Wang, Simulation of subcooled flow boiling in a micro-channel, Int. J. Refrig. 34 (2011) 781–795.
[37] R. Zhuan, W. Wang, Flow pattern of boiling in micro-channel by numerical simulation, Int. J. Heat Mass Transfer 55 (2012) 1741–1753.
[38] J.U. Brackbill, D.B. Kothe, C. Zemach, A continuum method for modeling surface tension, J. Comput. Phys. 100 (2) (1992) 335–354.
[39] D.L. Youngs, Time-dependent multi-material flow with large fluid distortion, in: K.W. Morton, M.J. Baines (Eds.), Numerical Methods for Fluid Dynamics, Academic Press, New York, 1982, pp. 273–285.
[40] R.N. Krishnan, S. Vivek, D. Chatterjee, S.K. Das, Performance of numerical schemes in the simulation of two-phase free flows and wall bounded mini channel flows, Chem. Eng. Sci. 65 (2010) 5117–5136.
[41] T. Taha, Z.F. Cui, Hydrodynamics of slug flow inside capillaries, Chem. Eng. Sci. 59 (2004) 1181–1190.
[42] D. Liu, S. Wang, Hydrodynamics of Taylor flow in noncircular capillaries, Chem. Eng. Process. 47 (2008) 2098–2106.
[43] V. Kumar, S. Vashisth, Y. Hoarau, K.D.P. Nigam, Slug flow in curved microreactors: hydrodynamic study, Chem. Eng. Sci. 62 (2007) 7494–7504.
[44] N. Shao, W. Salman, A. Gavriilidis, P. Angeli, CFD simulations of the effect of inlet conditions on Taylor flow formation, Int. J. Heat Fluid Flow 29 (2008) 1603–1611.
[45] D. Qian, A. Lawal, Numerical study on gas and liquid slugs for Taylor flow in a T-junction microchannel, Chem. Eng. Sci. 61 (2006) 7609–7625.
[46] Q. He, N. Kasagi, Phase-field simulation of small capillary-number two-phase flow in a microtube, Fluid Dyn. Res. 40 (2008) 497–509.
[47] Y. Chen, R. Kulenovic, R. Mertz, Numerical study on the formation of Taylor bubbles in capillary tubes, Int. J. Therm. Sci. 48 (2009) 234–242.
[48] R. Gupta, D.F. Fletcher, B.S. Haynes, On the CFD modeling of Taylor flow in microchannels, Chem. Eng. Sci. 64 (2009) 2941–2950.
[49] R.M. Santos, M. Kawaji, Numerical modeling and experimental investigation of gas–liquid slug formation in a microchannel T-junction, Int. J. Multiphase Flow 36 (2010) 314–323.
[50] H. Ganapathy, E. Al-Hajri, M.M. Ohadi, Phase field modeling of Taylor flow in mini/microchannels, Part II: Hydrodynamics of Taylor flow, Chem. Eng. Sci. 94 (2013) 156–165.
[51] H. Ganapathy, E. Al-Hajri, M.M. Ohadi, Phase field modeling of Taylor flow in mini/microchannels, Part I: Bubble formation mechanisms and phase field parameters, Chem. Eng. Sci. 94 (2013) 138–149.
[52] H. Ganapathy, E. Al-Hajri, M.M. Ohadi, Mass transfer characteristics of gas-liquid absorption during Taylor flow in mini/microchannel reactors. Chem. Eng. Sci. (2013). http://dx.doi.org/10.1016/j.ces.2013.06.005.
[53] E.W. Lemmon, M.L. Huber, M.O. McLinden, NIST Standard Reference Database 23: Reference Fluid Thermodynamic and Transport Properties-REFPROP, Version 9.0, National Institute of Standards and Technology, Standard Reference Data Program, Gaithersburg, 2010.
[54] N. Brauner, D. Moalem-Maron, Identification of the range of 'small diameter' conduits regarding two-phase flow pattern transition, Int. Commun. Heat Mass Transfer 19 (1992) 29–39.
[55] C. Fang, J.E. Steinbrenner, F. Wang, K.E. Goodson, Impact of wall hydrophobicity on condensation flow and heat transfer in silicon microchannels, J. Micromech. Microeng. 20 (2010) 0405018.
[56] C. Fang, C. Hidrovo, F. Wang, J. Eaton, K. Goodson, 3-D numerical simulation of contact angle hysteresis for microscale two phase flow, Int. J. Multiphase Flow 34 (2008) 690–705.
[57] M. Renardy, Y. Renardy, J. Li, Numerical simulation of moving contact line problems using a volume-of-fluid method, J. Comput. Phys. 171 (2001) 243–263.
[58] S. Thomas, A. Esmaeeli, G. Tryggvason, Multiscale computations of thin films in multiphase flows, Int. J. Multiphase Flow 36 (2010) 71–77.
[59] F.P. Bretherton, The motion of long bubbles in tubes, J. Fluid Mech. 10 (1961) 166–188.
[60] P. Aussillous, D. Quere, Quick deposition of a fluid on the wall of a tube, Phys. Fluids 12 (10) (2000) 2367–2371.
[61] J.W. Coleman, S. Garimella, Two-phase flow regimes in round, square and rectangular tubes during condensation of refrigerant R134a, Int. J. Refrig. 26 (2003) 117–128.
[62] H.Y. Wu, P. Cheng, Condensation flow patterns in silicon microchannels, Int. J. Heat Mass Transfer 48 (2005) 2186–2197.
[63] J.S. Hu, C.Y.H. Chao, An experimental study of the fluid flow and heat transfer characteristics in micro-condensers with slug bubbly flow, Int. J. Refrig. 20 (2007) 1309–1318.
[64] H. Wu, M. Yu, P. Cheng, X. Wu, Injection flow during steam condensation in silicon microchannels, J. Micromech. Microeng. 17 (2007) 1618–1627.
[65] W. Zhang, J. Xu, J.R. Thome, Periodic bubble emission and appearance of an ordered bubble sequence (train) during condensation in a single microchannel, Int. J. Heat Mass Transfer 51 (2008) 3420–3433.
[66] C. Fang, M. David, F. Wang, K.E. Goodson, Influence of film thickness and cross-sectional geometry on hydrophilic microchannel condensation, Int. J. Multiphase Flow 36 (2010) 608–619.
[67] S.-M. Kim, J. Kim, I. Mudawar, Flow condensation in parallel micro-channels – Part 1: Experimental results and assessment of pressure drop correlations, Int. J. Heat Mass Transfer 55 (2012) 971–983.
[68] L. Zhang, E.N. Wang, K.E. Goodson, T.W. Kenny, Phase change phenomena in silicon microchannels, Int. J. Heat Mass Transfer 48 (2005) 1572–1582.
[69] W.H. McAdams, W.K. Woods, L.C. Heroman, Vaporization inside horizontal tubes. II: Benzene–oil mixture, Trans. ASME 64 (1942) 193–200.
[70] K. Mishima, T. Hibiki, Some characteristics of air–water two-phase flow in small diameter vertical tubes, Int. J. Multiphase Flow 22 (1996) 703–712.
[71] H.J. Lee, S.Y. Lee, Pressure drop correlations for two-phase flow within horizontal rectangular channels with small heights, Int. J. Multiphase Flow 27 (2001) 783–796.
[72] V.G. Nino, E.W. Jassim, P.S. Hrnjak, T.A. Newell, Flow regime based model for pressure drop predictions in microchannels, University of Illinois at Urbana-Champaign, 2005 ACRC TR-242.
[73] Y.W. Hwang, M.S. Kim, The pressure drop in microtubes and the correlation development, Int. J. Heat Mass Transfer 49 (2006) 1804–1812.
[74] W. Li, Z. Wu, A general correlation for adiabatic two-phase pressure drop micro/mini-channels, Int. J. Heat Mass Transfer 53 (2010) 2732–2739.
[75] W. Zhang, T. Hibiki, K. Mishima, Correlations of two-phase frictional pressure drop and void fraction in mini-channel, Int. J. Heat Mass Transfer 53 (2010) 453–465.
[76] S.-M. Kim, I. Mudawar, Universal approach to predicting two-phase frictional pressure drop for adiabatic and condensing mini/micro-channel flows, Int. J. Heat Mass Transfer 55 (2012) 3246–3261.
[77] M.M. Shah, A general correlation for heat transfer during film condensation inside pipes, Int. J. Heat Mass Transfer 22 (1979) 547–556.
[78] M.K. Dobson, J.C. Chato, Condensation in smooth horizontal tubes, J. Heat Transfer 120 (1998) 193–213.
[79] M.M. Shah, An improved and extended general correlation for heat transfer during condensation in plain tubes, HVAC&R Res. 15 (5) (2009) 889–913.
[80] J.S. Shin, M.H. Kim, An experimental study of condensation heat transfer inside a mini-channel with a new measurement technique, Int. J. Multiphase Flow 30 (2004) 311–325.
[81] M. Derby, H.J. Lee, Y. Peles, M.K. Jensen, Condensation heat transfer in square, triangular, and semi-circular mini-channels, Int. J. Heat Mass Transfer 55 (2012) 187–197.
[82] S.-M. Kim, I. Mudawar, Flow condensation in parallel micro-channels – Part 2: Heat transfer results and correlation technique, Int. J. Heat Mass Transfer 55 (2012) 984–994.
[83] W.-W.W. Wang, T.D. Radcliff, R.N. Christensen, A condensation heat transfer correlation for millimeter-scale tubing with flow regime transition, Exp. Therm. Fluid Sci. 26 (2002) 473–485.